

Article

# Effect of Steel Substrates on the Formation and Deuterium Permeation Resistance of Aluminide Coatings

Xin Xiang \* , Feilong Yang, Guikai Zhang and Xiaolin Wang

Institute of Materials, China Academy of Engineering Physics, Jianguo 621908, China; yangfeilong@caep.cn (F.Y.); zhangguikai@caep.cn (G.Z.); xlwang@caep.cn (X.W.)

\* Correspondence: xiangxin-7s@caep.cn; Tel.: +86-816-362-6480; Fax: +86-816-362-5900

Received: 28 November 2018; Accepted: 31 January 2019; Published: 4 February 2019



**Abstract:** The effect of steel substrates on the formation and deuterium permeation resistance of aluminide coatings for tritium permeation barrier applications was investigated. It was found that the average thickness and crystal structure of electrodeposited Al coatings varied with Cr steel substrates. After aluminization in vacuum, significant differences existed in the composition and thickness of (Fe,Cr)<sub>2</sub>Al<sub>5</sub>-type aluminide layers formed on different Cr steel substrates, in which the alloying element Cr from steel substrates was involved. Thereafter, the scale microstructural feature and thickness also changed with the Cr steel substrate after selective oxidation in an Ar gas stream. Consequently, the deuterium permeation resistance of the formed aluminide tritium permeation barriers (TPBs) differed by steel substrates, indicating that the substrate effect existed in aluminide TPB coatings and thus could have a significant influence on the formation and eventual performance of aluminide TPBs.

**Keywords:** substrate effect; aluminide coating; formation; deuterium permeation resistance

## 1. Introduction

The test blanket module (TBM) is the key component for testing the feasibility of tritium self-sufficiency and energy extraction in the international thermonuclear experimental reactor (ITER). However, the radioactive tritium permeating into and through structural materials in TBMs can result in fuel loss, material embrittlement, and environmental contamination [1]. From the view of economy, safety, and environmental preservation, structural materials in the blanket and auxiliary tritium handling systems must have the lowest tritium permeability. A thin coating layer as a tritium permeation barrier (TPB) is commonly employed to minimize tritium permeation through structural materials to the coolant, environment, and other functional components in TBMs [2–4]. Therefore, the application of TPBs is essential for tritium self-sufficiency and environmental safety in the blanket.

Among various developed TPB coatings, an aluminide coating typically composed of an inner Fe–Al transition layer with an outer Al<sub>2</sub>O<sub>3</sub> film has been selected as the first choice of TBM TPBs by China, Europe, India, and the United States for its high permeation reduction factor (PRF), metallurgical bonding, excellent compatibility, and self-healing [5–7]. Recently, although Pedraza et al. [8] have reported that there is a significant mismatch between aluminide coatings and steel substrates, which could lead to tensile cracks, aluminide coatings still showed good stability after steam exposure for 2000 h. However, aluminide TPBs often exhibit much lower actual performance than predicted based on bulk material properties [9,10]. One of the most possible reasons may be alloying elements from the steel substrate or Al source, and microstructures of substrate materials such as crystal and metallographic structures may also exert some influence on coating formation and performance [10–13],

which could be called an alloying effect including a substrate effect and a doping effect in aluminide coatings [14]. The latter originates from doped species in the Al source or predeposited species on the substrate [14]. Presently, however, aluminide TPB studies are mainly devoted to preparation technique and performance optimization. For the alloying effect, especially the substrate effect, some work has been conducted on aluminide coatings on Ni-based superalloys [15], while for aluminide coating on steels, much less work has been involved. In fact, the alloying effect is very important for preparation technique optimization and coating structure design, and thus is a substantial fundamental issue in the practical preparation and application of aluminide TPBs on steels.

In the blanket and auxiliary tritium systems in fusion reactors, FeCr base steels are the mainly used structural materials. Crystal structure, metallographic phase, and the content and species of alloying elements vary with steel types [16–22]. The formation and tritium tolerance of aluminide TPBs formed on various types of steels are expected to be different because of different steel substrates. It has already been noted that the high temperature steam oxidation resistance of aluminized HCM12A steel was better than P-91 steel, and the reason was attributed to the different Cr content in the two steel substrates [23]. Soliman et al. [24] found that with an increase in C content from 0.22 to 0.44 wt%, the rate constant of high-temperature oxidation decreased by nearly one order of magnitude in aluminized carbon steels. Moreover, compared to the aluminide layers formed on the four different steel substrates Eurofer 97, DIN1.4914, MANET II, and HR-2, significant differences could be observed for the layer structures, phases formed, defects, and interface features, etc. [3,25–27]. Though different preparation techniques, e.g., hot-dipping aluminization (HDA), pack cementation (PC), plasma spraying (PS), and electrochemical deposition (ECD), have been adopted for these steels, the intrinsic properties of steel substrates could have some influence on the formation of aluminide coatings [8,15], since the alloying elements and metallographic phases differ a lot [3,25–27].

On the other hand, the addition of 1 wt % C to Fe-16 wt % Al has enabled the formation of a cementite-like carbide phase, i.e.,  $\text{Fe}_3\text{AlC}_{0.5}$  in Fe<sub>3</sub>Al-based alloys, resulting in reductions of H permeability and a diffusion coefficient up to two orders of magnitude [28]. Moreover, the hydrogen permeability of proton-irradiated EP-838 steels lowered by almost one order of magnitude after Ce doping [29]. It can thus be inferred that properties of steel substrates themselves and alloying elements (contained or doped) may exert some influence on the formation and performance of aluminide coatings, i.e., the alloying effect may exist in aluminide TPB coatings. However, the alloying effect, especially the substrate effect, in aluminide TPBs formed on steel substrates has been rarely involved at present. Therefore, in the present work, aluminide TPB coatings were prepared on three types of Cr steels (1Cr8, 1Cr13, and 1Cr15), and subsequently the effect of steel substrates on the formation and deuterium permeation resistance of aluminide coatings was investigated to clarify the substrate effect in aluminide TPBs. The results are anticipated to be instructive for the selection, development, and optimization of the preparation technique of aluminide TPBs.

## 2. Experimental

### 2.1. Materials and Al Electrodeposition

The samples used were commercial Cr steels with different metallographic phases and nominal compositions, as shown in Table 1, and the corresponding XRD patterns are illustrated in Figure 1. Before Al electrodeposition, steel samples (20 mm × 20 mm × 2 mm) were grinded, polished, ultrasonically cleaned in acetone and ethanol in turn, and then dried in air and transferred to an Ar protected glove box. The ECD technique, i.e. ionic liquid (IL) plating [14], was employed to prepare Al coatings on Cr steel substrates. The electrolyte was synthesized with 1-ethyl-3-methylimidazolium chloride (EMIC, 64.5 wt %, Zhejiang Univ., Hangzhou, China) and anhydrous aluminum chloride ( $\text{AlCl}_3$ , 35.5 wt %, Sigma-Aldrich, St. Louis, MO, USA). The Al electrodeposition was carried out in a two-electrode setup (Cr steel sample as cathode, and 99.999% purity Al wire as anode) with the constant current mode (10 mA/cm<sup>2</sup>) for 1–2 h at room temperature in the Ar protected glove box. Prior

to the Al electrodeposition, both the cathode and anode were ultrasonically cleaned in phosphoric acid, methanol, acetone, and ethanol successively to remove surface oxides and organic impurities, and were then dried in the air.

**Table 1.** The nominal chemical composition and metallographic phase of Cr steels.

Steel Type	Chemical Composition, wt%							Metallographic Phase
	Cr	Ni	Mn	C	P	S	Fe	
1Cr8	10.0	0.21	0.52	0.15	0.03	0.03	Balance	Martensite
1Cr13	13.0	0.60	0.95	0.15	0.03	0.03	Balance	Martensite
1Cr15	16.0	0.60	0.95	0.15	0.03	0.03	Balance	Ferrite

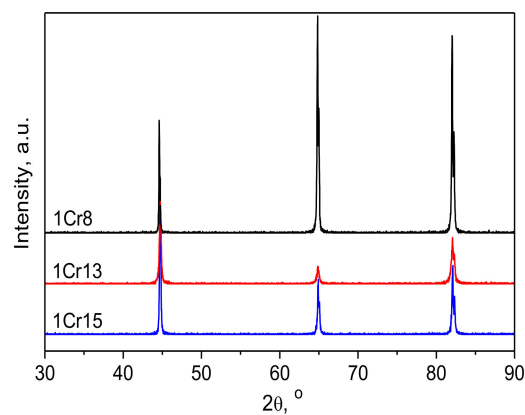


**Figure 1.** XRD patterns for Cr steels.

## 2.2. Aluminization and Oxidation

The preparation of aluminide TPBs commonly involves two steps of aluminization and oxidation to form an inner aluminized coating (Fe–Al transition layer) with an outer oxide film ( $\text{Al}_2\text{O}_3$ ) [25,30]. Aluminized coatings were obtained by heating Al electrodeposited samples in a vacuum tubular furnace ( $\sim 10^{-2}$  Pa) at 500 °C for 4 h and then by cooling in the furnace. Mainly the inward diffusion of Al atoms from the predeposited Al coatings into steel substrates occurred [31]. Selective oxidation of the aluminized coatings took place in the tubular furnace at 700 °C for 120 h in an Ar gas stream (99.99%,  $1.2 \times 10^5$  Pa, 20–30 ppmv  $\text{O}_2$ ). It should be noted that such a condition for selective oxidation is too harsh for reduced activation ferritic/martensitic steels as the candidate structural materials in fusion reactors, for which the optimal TPB preparation technique needs to be further investigated in the future.

## 2.3. Characterization

The surface topographies and cross-section features of the Al electrodeposited, aluminized, and selectively oxidized Cr steel samples were observed by scanning electronic microscope (SEM, EM8000F, KYKY, Beijing, China). Since the interfaces between Al or aluminide layers and steel substrates were not flat and straight, the statistical averages of coating thicknesses were determined. The chemical composition and phase constituent of formed coatings were identified by a combination of energy dispersive spectroscopy (EDS, area analysis mode, Octane SDD, EDAX, Mahwah, NJ, USA) and X-ray diffraction spectrum (XRD, Cu  $K\alpha$ , DX-2700BH, Haoyuan, Dandong, China). The chemical states and depth profiles of Fe, Al, Cr, and O in scales were detected by X-ray photoelectron spectroscopy (XPS, ESCA LAB 250, Thermo Fisher, MA, USA), and the film thickness by the technique of reflection spectrum (RS, FX2000, ideaoptics, Shanghai, China), in which the thickness is determined by the amplitude and periodicity of the reflectance on the film surface [32].

PRF is one of the most important performance indexes for TPBs, and is obtained by the ratio of hydrogen isotopic permeability of coated and bare samples. In order to obtain a more accurate PRF, at least three samples ( $\phi 32 \times 1$  mm) coated with aluminide TPBs for each type of Cr steel substrate were measured, and then the average PRFs at each temperature were calculated. The specific apparatus and process for PRF measurements have been described earlier by Zhang et al. [25]. Deuterium (99.99%) was used for permeation tests, and the upstream pressure was 100 kPa, while the downstream was connected to the vacuum system. The test temperatures were set at 552, 605, 652, and 700 °C, and then the correlation of temperature permeability could be plotted.

### 3. Results and Discussion

#### 3.1. Electrodeposition of Al Coating

From Figure 1, it can be seen that three peaks located at 45°, 65°, and 82° were present for these three types of steels. For 1Cr8 steel, peaks at 65° and 82° were the most prominent, while for 1Cr13 and 1Cr15 steels, there were peaks at 45° and 82°. Moreover, for 1Cr13 steel, the intensity of the peak at 65° was much smaller than the other two peaks, while for 1Cr8 and 1Cr15 steels, the smallest intensity peaks (located at 45° and 65°, respectively) could be comparable to the other two ones. Obviously, the crystal structures of these three types of steels are different. Actually, as common industry-used steels, the crystal types of 1Cr8, 1Cr13, and 1Cr15 steels are definitely body-centered tetragon (BCT), BCT, and body-centered cubic (BCC), respectively.

After the same procedures of surface preparation and plating pretreatment, Al coatings were electrodeposited on three types of Cr steel substrates. As shown in Figure 2a–c, dense Al deposits formed on Cr steel samples without observable defects, such as voids and cracks, after 1 h of IL plating. Similar surface morphologies of Al layers could be observed on different Cr steel substrates. However, the corresponding XRD patterns were a little different, as shown in Figure 2d. For 1Cr8 steel, peaks (200) and (220) were the most prominent, while for 1Cr13 and 1Cr15 steels, they were peaks (111) and (200). Nevertheless, no preferential growth of Al grains was obviously observed in these Cr steels, as earlier reported on 321 steel workpieces [25]. Moreover, prior to Al electrodeposition, no obvious orientation existed in these three steels either (Figure 1). By comparison, 321 steel has a different crystal structure (face-centered cubic (FCC)) and metallographic phase (austenite) with a higher Cr content (18.0 wt%), while the Cr steels used in this work are BCT- (1Cr8, 1Cr13) or BCC-structured (1Cr15) and martensitic- (1Cr8, 1Cr13) or ferritic-phased (1Cr15). Therefore, it could be inferred that the difference in material properties, including crystal structure, metallographic phase, and alloying element content, for different steel substrates could have resulted in the difference in Al coatings shown in Figure 2d. The property difference of Cr steels may also have affected the electrodeposition efficiency, nucleation, and growth mechanism of Al layers on different substrates. In a word, Cr steel substrates themselves may have an impact on the Al electrodeposition process.

The cross-section features of Al coatings formed on Cr steel substrates are shown in Figure 3a–c. Continuous pure Al (Figure 3d) layers with average thicknesses of  $5.0 \pm 0.6$ – $12.5 \pm 0.9$   $\mu\text{m}$  were observed, showing that Al layers were well adhered to steel substrates. Similarly to Figure 2, a slight difference could be found for the topography of formed Al layers in Figure 3. However, remarkable discrepancies occurred in the thickness of Al layers. The average Al thickness formed on 1Cr8 steel ( $\sim 12.5$   $\mu\text{m}$ ) was about two times larger than 1Cr15 steel ( $\sim 5.0$   $\mu\text{m}$ ). Moreover, the average Al thicknesses were arranged in an order of  $1\text{Cr}8 > 1\text{Cr}13 > 1\text{Cr}15$ , as if the Al thickness decreased with the Cr content in steel substrates. Since the same surface pretreatment was conducted to obtain a similar surface condition, including roughness, for the three types of Cr steel samples before plating, and the Al coating parameters were also identical, the thickness of as-deposited Al layers should have thus only been affected by properties of steel substrates. The differences in material properties in Cr steels would have caused a variation in Al electrodeposition efficiency on different substrates, leading to inhomogeneous thicknesses of Al layers formed. It may have been a coincidence that the thickness

of the electrodeposited Al layer was reduced with increasing Cr content, which may have originated from the crystal structure and metallographic phase of steels, since Cr was not involved in the process of electrodeposition (Figure 3d). In a word, it is certain that the steel substrate had an influence on the process of Al electrodeposition.

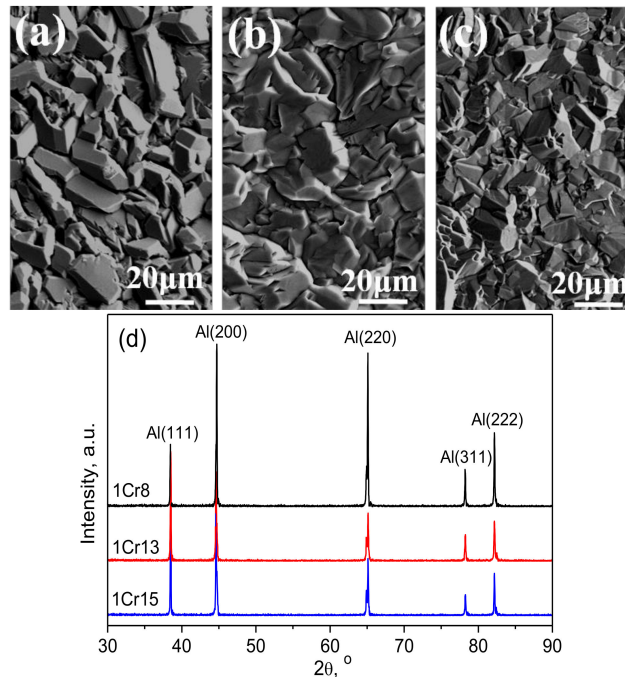


**Figure 2.** Surface topographies of Al coatings formed on (a) 1Cr8, (b) 1Cr13, and (c) 1Cr15 steel substrates and (d) the corresponding XRD patterns after 1 h of ionic liquid (IL) plating.

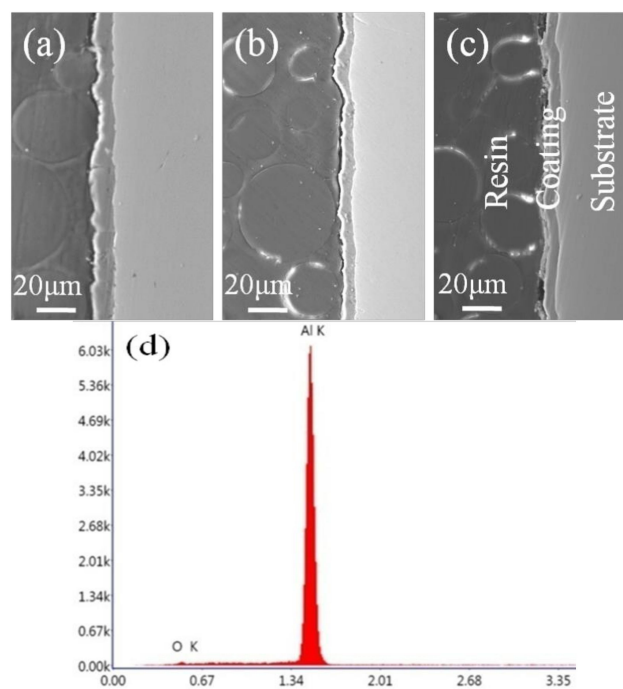


**Figure 3.** Cross-section features of Al coatings formed on (a) 1Cr8, (b) 1Cr13, and (c) 1Cr15 steel substrates and (d) the corresponding energy dispersive spectroscopy (EDS) spectrum after 1 h of IL plating.

### 3.2. Aluminization of Al Coating

The process of aluminization is forming a transition layer of (Fe, Al) solid solution and/or Fe–Al metallic compounds on the substrate surface via interdiffusion between Al atoms from a certain Al source and Fe atoms from steel substrates [14]. After 500 °C, 4 h heat treatment in vacuum, single-layered  $\text{Fe}_2\text{Al}_5$ -type aluminide coatings formed on these three types of Cr steel substrates, as shown in Figure 4. The single-layered aluminide structures were different from earlier reported two- or three-layered structures [12,25,32–34], and may have originated from the much lower heat treatment temperature and shorter time adopted in this work. The relative chemical compositions and possible phases for aluminide coatings are listed in Table 2. Since no Cr–Al intermetallics were recognized, the formed aluminide coatings were identified as  $(\text{Fe,Cr})_2\text{Al}_5$  layers by combining XRD patterns with EDS results, similarly to the case of aluminized P-91 and HCM12A steels at 550 °C [23]. Gregoire et al. [35] have reported that  $\text{Al}_x\text{Cr}_y$  intermetallic compounds could not form by mixing Al and Cr microparticles at temperatures lower than  $637 \pm 2$  °C. At 500 °C, a phase of  $\text{Al}_{11}\text{Cr}_2$  could form only by hot isostatic pressing of 55Al45Cr powders [36]. Obviously, during the aluminization in the present work, no Al–Cr intermetallics were created, and Cr atoms from the steel substrates could dissolve in the formed  $\text{Fe}_2\text{Al}_5$  to generate a  $(\text{Fe,Cr})_2\text{Al}_5$  solid solution. In short, the main alloying element Cr was involved in the thermal diffusion process of Fe and Al atoms during aluminization. A similar phenomenon was also observed in hot-dipped aluminide Cr–Mo steels [37]. Besides, the Cr content in aluminide coatings increased with the Cr concentration in steel substrates, which was quite expected. The solid state reactive diffusion between Fe and Al at 823–913 K for up to 120 h [38] showed that the interdiffusion coefficient of Al was much greater than Fe and Fe–Al intermetallics. Therefore, Al atoms diffused inwardly during the 500 °C, 4 h aluminization, yet there was barely any diffusion of Fe and Cr, resulting in the formation of aluminide layers with higher Cr content for higher Cr steel. That is, the alloying element Cr from steel substrates was passively involved in the aluminization process for the deposited Al coatings on Cr steel substrates.

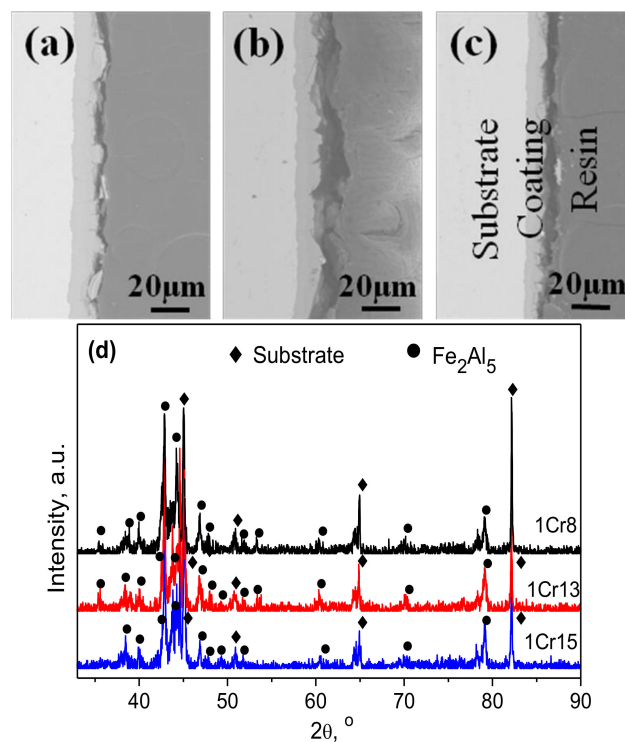


**Figure 4.** Cross-section images of aluminide coatings formed on Al deposited (a) 1Cr8, (b) 1Cr13, and (c) 1Cr15 steel substrates and (d) the corresponding XRD patterns after 500 °C, 4 h heat treatment in vacuum.

**Table 2.** EDS results of aluminide coatings formed on Al-deposited Cr steel substrates after 500 °C, 4 h heat treatment in vacuum.

Steel Type	Relative Chemical Composition, at %			Possible Phase
	Al	Fe	Cr	
1Cr8	70.48	26.17	3.35	(Fe,Cr) <sub>2</sub> Al <sub>5</sub>
1Cr13	71.36	24.10	4.54	(Fe,Cr) <sub>2</sub> Al <sub>5</sub>
1Cr15	70.39	24.58	5.03	(Fe,Cr) <sub>2</sub> Al <sub>5</sub>

As for the cross-section features, it was found that the average thicknesses of the aluminide coatings formed on these three types of Cr steel substrates were about  $7.1 \pm 0.8$ – $14.6 \pm 0.5$   $\mu\text{m}$  (Figure 4a–c), thicker than the corresponding initial Al layers (Figure 3a–c) and resulting from the inward diffusion of Al atoms during aluminization [38]. Moreover, such thicknesses shared the same rank order as those of the previous Al coatings deposited on Cr steel substrates, i.e., 1Cr8 > 1Cr13 > 1Cr15, and the average thickness of the aluminide layer formed on 1Cr8 (~14.6  $\mu\text{m}$ ) steel was still two times larger than that on 1Cr15 (~7.1  $\mu\text{m}$ ), which also seemed like the aluminide layer thickness decreased with the Cr content in steel substrates. However, a greater initial Al coating thickness did not necessarily imply a thicker aluminide coating after annealing. On one hand, Cr could act as a diffusion barrier for the Al ingress [39]. Therefore, it seems very reasonable that the aluminide layer formed on the 1Cr15 steel was thinner than 1Cr13 and 1Cr8 steels due to its higher Cr content. On the other hand, the metallographic structure of 1Cr15 steel is ferrite, while it is martensite for 1Cr8 and 1Cr13 steels. It is known that for martensite, C is supersaturated and dissolved into  $\alpha$ -Fe, resulting in the formation of a highly strained BCT crystal structure, but for ferrite, C is interstitially dissolved in  $\alpha$ -Fe, and thus the C content is very small and the crystal remains BCC-structured. Earlier experimental and theoretical studies have shown that both interdiffusion and surface diffusion in metals can be enhanced by strain [40–42]. From this point, more readiness for Al diffusion into 1Cr8 and 1Cr13 steels than into 1Cr15 steel was quite expected. Therefore, there must have been a substrate effect during aluminization, resulting not only from the Cr content in steel substrates, but also from the material properties of these substrates, including the crystal structure, metallographic phase, and even other alloying elements such as C, Si, Mn, and Ni (although not recognized in this work).

### 3.3. Oxidation of Aluminide Coating

To achieve the best tritium permeation resistance, the aluminide coatings have to be selectively oxidized to form a thin layer of Al<sub>2</sub>O<sub>3</sub> film, since the main functional component of aluminide TPBs is the outer Al<sub>2</sub>O<sub>3</sub> film (other than the inner Fe–Al transition layer) [43]. Experimentally, selective oxidation is often realized via control of the content of alloying elements and oxygen pressure, etc. [44,45]. The latter was adopted in this work. After selective oxidation in the tubular furnace at 700 °C for 120 h in an Ar gas stream, scales were created on the aluminide coating of each Cr steel sample. Take 1Cr13 as an example: XPS depth profiles (Figure 5) showed that there were mainly signals of Al and O on the scale surface when the etching time was less than 5 min, yet nearly no Fe and Cr peaks appeared, suggesting that pure Al<sub>2</sub>O<sub>3</sub> films were created on the sample surfaces (that is, selective oxidation occurred). With the increase in etching time, the signal of the Al oxide state (~83.7 eV) gradually decreased, while the metallic state (around 75 eV) increased (Figure 5c). When the etching time reached 10 min, the oxide peak of Al almost disappeared, and metallic states of Fe and Cr emerged on the surface (Figure 5a–c). Meanwhile, the oxide state (586.1 and 576.4 eV) of Cr also appeared (Figure 5b), indicating that a small amount of Cr<sub>2</sub>O<sub>3</sub> formed, besides Al<sub>2</sub>O<sub>3</sub>. On the other hand, the relative content of O started to decrease dramatically after etching for 2 min, while the Fe content got a significant increase, accompanied by a mild decrease in Al content and an increase in Cr content, as shown in Figure 5e. Since XPS is a semiquantitative technique, it thus can be estimated that from the outer surface to the inner surface, the surface coatings could be divided

into three zones, i.e.,  $\text{Al}_2\text{O}_3$ ,  $(\text{Al,Cr})_2\text{O}_3/(\text{Fe,Cr})_x\text{Al}_y$ , and  $(\text{Fe,Cr})_x\text{Al}_y$  layers. The actual phase of scales could be identified as  $\gamma\text{-Al}_2\text{O}_3$  by XRD (Figure 5f), consistent with the cases performed on 321 steel workpieces [25]. After all, selective oxidation was only conducted at  $700\text{ }^\circ\text{C}$  in the present work. Such a low temperature could not enable the formation of a more stable alumina, i.e.,  $\alpha\text{-Al}_2\text{O}_3$ , for which the formation temperature is usually higher than  $1000\text{ }^\circ\text{C}$  [46], much higher than the service temperature ( $\sim 500\text{ }^\circ\text{C}$ ) of structural materials in fusion reactors [4]. Actually,  $\gamma\text{-Al}_2\text{O}_3$  forming at  $700\text{ }^\circ\text{C}$  is enough for hydrogen resistance, according to our previous studies [25,32]. Moreover, during the long-time high-temperature selective oxidation, phase transitions took place. Specifically, the inner part of the pre-formed  $(\text{Fe,Cr})_2\text{Al}_5$  layer gradually converted to  $(\text{Fe,Cr})_x\text{Al}_y$ , since Al atoms could diffuse more deeply into the steel substrate at a higher temperature of  $700\text{ }^\circ\text{C}$ , and thus the relative content of Al over Fe and Cr decreased, leading to the formation of Al-depleted intermetallics such as  $(\text{Fe,Cr})_3\text{Al}$ ,  $(\text{Fe,Cr})\text{Al}_2$ , and  $(\text{Fe,Cr})\text{Al}$  or their mixtures, labeled as  $(\text{Fe,Cr})_x\text{Al}_y$  on the whole. Meanwhile, phase transitions also occurred for the outer part of the pre-formed  $(\text{Fe,Cr})_2\text{Al}_5$  layer, generating various Al-depleted  $(\text{Fe,Cr})\text{-Al}$  intermetallics, also labeled as  $(\text{Fe,Cr})_x\text{Al}_y$ . At the same time, for more readiness of oxidation under the condition of more extreme low oxygen partial pressure than Fe [47], Al and Cr atoms from the very near outer surface started to be oxidized, as shown in Figure 5b,c. Only  $\text{Al}_2\text{O}_3$  scales could be created with the extending oxidation duration, because Al atoms have a better affinity with O than Cr atoms under this O condition [47]. As a result, a sandwich-like structure was created on steel substrates (Figure 5e). In a word, Cr atoms from steel substrates were involved in the process of the selective oxidation, may exerting an influence on the transition layers of  $\text{Al}_2\text{O}_3/\text{Fe-Al}$  TPB coatings.

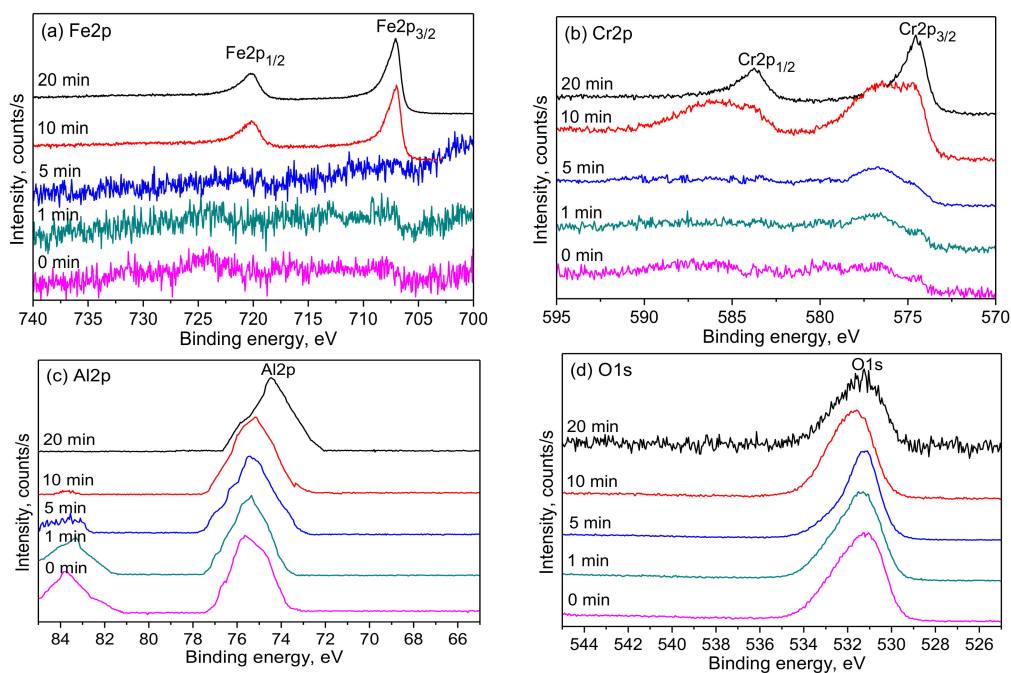
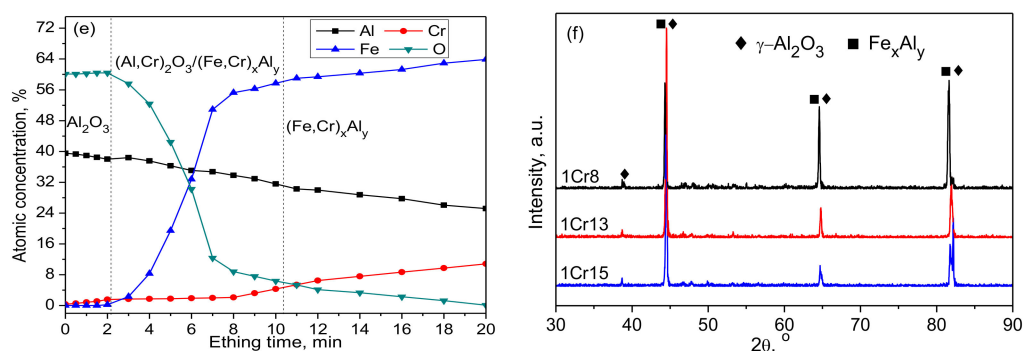
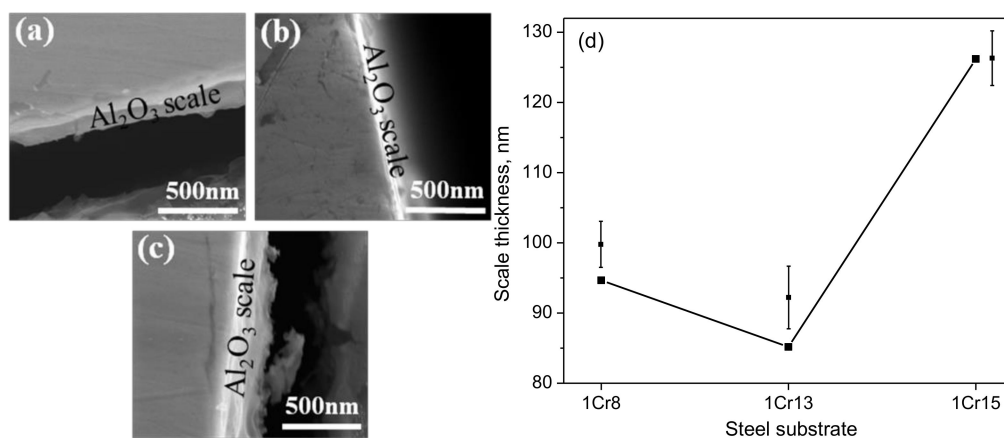


Figure 5. Cont.



**Figure 5.** Depth profiles of (a) Fe, (b) Cr, (c) Al, (d) O, and (e) the relative atomic contents for scales formed on aluminide 1Cr13 steel; and (f) XRD patterns for aluminide coatings formed on Cr steel substrates after 700 °C, 120 h selective oxidation in an Ar gas stream.

However, the scales formed exhibited irregular growth features (Figure 6a–c), and the thicknesses deviated and thus were difficult to determine from the cross-section features. Anyway, it could be roughly estimated that the average thicknesses of scales formed were in an order of 1Cr15 > 1Cr8 > 1Cr13. Since the scales formed on aluminide coatings are usually very thin (less than 1 μm) [25, 32], the RS technique [25,32] is commonly adopted to determine scale thickness. According to the amplitude and periodicity of RS spectra [25], the average thicknesses of Al<sub>2</sub>O<sub>3</sub> scales formed on different Cr steel samples were estimated, about 85.18 ± 0.35–126.22 ± 0.33 nm. Moreover, the average thicknesses of the Al<sub>2</sub>O<sub>3</sub> scales were arranged in an order of 1Cr15 > 1Cr8 > 1Cr13 (Figure 6d), consistent with the cross-section observations (Figure 6a–c), yet different from the previous thickness orders of deposited Al layers and aluminide coatings, i.e., 1Cr8 > 1Cr13 > 1Cr15 (Figures 3 and 4). At a selective oxidation temperature of 700 °C, interdiffusions take place among Fe, Cr, and Al atoms [35,48], resulting in the alteration of the chemical environment of Al atoms from the outer surface of previously formed (Fe,Cr)<sub>2</sub>Al<sub>5</sub> layers, which consequently has an impact on the subsequent selective oxidation process [44,47]. On the other hand, significant differences existed in the microstructures and compositions of the formed aluminide layers on these three steel substrates (Figure 4 and Table 2), which could also have exerted an influence on the nucleation and growth behaviors of scales. It can be seen that the formation of Al<sub>2</sub>O<sub>3</sub> scales was a rather complex process, and thus was difficult to predict by a single factor. Maybe the scale thickness order is an illustration of this. Obviously, more data are needed to verify the substrate effect in the process of selective oxidation.



**Figure 6.** Cross-section features of scales formed on aluminized (a) 1Cr8, (b) 1Cr13, and (c) 1Cr15 steel samples after 700 °C, 120 h selective oxidation in an Ar gas stream, and (d) the corresponding scale thicknesses determined by a reflection spectrum (RS) (the error bar is enlarged by about 10×).

### 3.4. Deuterium Permeation Resistance of Aluminide TPBs

As stated above, the substrate effect exists in the formation of aluminide TPB coatings and plays a role in the process of Al electrodeposition, aluminization, and even selective oxidation. Whether the substrate effect also has an impact on the performance of aluminide TPBs thus needs to be concerned. Therefore, the deuterium permeation flux ( $J$ ) of these three types of Cr steel samples at different temperatures before and after coating with aluminide TPBs was tested, as shown in Figure 7. It can be seen that the deuterium permeation flux of each Cr steel substrate sample increased almost linearly with temperature (Figure 7a). As for different Cr steel samples, the increase extent of permeation flux with temperatures differed a lot. At 552 °C, the deuterium permeation flux of the 1Cr15 steel sample was the highest, while that of 1Cr8 steel was the lowest and that of 1Cr13 steel was placed in the middle. With the increase in temperatures, the deuterium permeation flux of the 1Cr13 steel sample increased rapidly, much higher than that of the 1Cr8 and 1Cr15 ones, about twice higher at 652 °C. For the latter two Cr steel samples, when the temperature was lower than 605 °C, the deuterium permeation flux of 1Cr15 steel was slightly higher than that of 1Cr8 steel and a little lower than 1Cr8 steel at higher temperatures. The activation energies for deuterium permeation through 1Cr8, 1Cr13, and 1Cr15 steel substrates at the temperature range of 552–700 °C could be obtained by Arrhenius fittings (Figure 7b), that is, 37.22, 71.52, and 28.88 kJ/mol, respectively. Obviously, there was a substantial divergence in the deuterium permeation of different Cr steel samples. That is, the substrate material properties (Cr content, crystal structure, metallographic phase, etc.) had an impact on the deuterium permeation, leading to the anticipation that the Cr steel substrates themselves would play a role in the deuterium permeation resistance of the subsequently prepared aluminide TPB barriers.

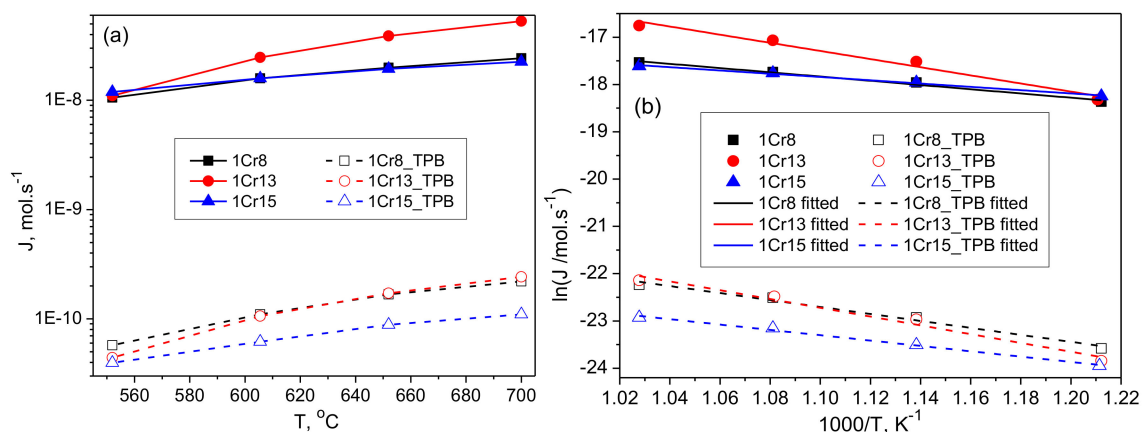


**Figure 7.** (a) Deuterium permeation flux of Cr steel samples before and after coating with aluminide tritium permeation barriers (TPBs) and (b) the corresponding Arrhenius fittings.

After coating with aluminide TPBs, the deuterium permeation flux at 552–700 °C of each Cr steel sample was remarkably reduced, up to two orders of magnitude, as shown in Figure 7a, indicating that the prepared aluminide TPBs were effective in deuterium permeation resistance, which could be attributed to the formation of outer scales. Generally speaking, for FeAl/Al<sub>2</sub>O<sub>3</sub>-type aluminide TPBs, the hydrogen PRF of an outer Al<sub>2</sub>O<sub>3</sub> scale under a convenient service condition is much higher than that of the inner transition FeAl layer, which has been verified both in experimental and theoretical studies [1,43]. From the view of PRF, the deuterium PRF for 1Cr8 steel samples at 552, 605, 652, and 700 °C were 185, 144, 118, and 110, respectively; for 1Cr13 steel samples, they were 250, 233, 226, and 218; and for 1Cr15, they were 300, 240, 220, and 204. In contrast, the deuterium permeation resistance of aluminide TPBs on 1Cr8 steel samples was much less effective than that on 1Cr13 and 1Cr15 steel samples at the same temperatures. For the last two types of Cr steels, the deuterium permeation resistance of aluminide TPBs on 1Cr13 steel samples was not as effective as that on 1Cr15 steel samples at temperatures lower than 605 °C, while at temperatures

higher than 605 °C, opposite results emerged. On the other hand, after coating with aluminide TPB, the deuterium permeation activation energies were 61.27, 77.16, and 46.98 kJ/mol for 1Cr8, 1Cr13, and 1Cr15 steels by the Arrhenius fittings, respectively, much higher than for uncoated ones, also showing the permeation resistance of aluminide TPBs. It thus can be seen that there were significant divergences in the deuterium permeation resistance of aluminide TPBs on different Cr steel substrates. That is, the substrate effect existed in aluminide TPBs, exerting an influence on the deuterium permeation resistance.

It should be noted that a conflict seemed to be present between the deuterium resistance (Figure 7a) and scale thicknesses (Figure 6d). For example, the deuterium permeation resistance of aluminide TPBs on 1Cr8 steel was much less effective than that on 1Cr13 steels, according to Figure 7a. However, from Figure 6d, it can be seen that the thickness of Al<sub>2</sub>O<sub>3</sub> on 1Cr8 steel was larger than that on 1Cr13 steel. Generally speaking, for a special steel type, it is indeed the case that the deuterium PRF increases with the scale thickness, and then reaches almost a constant if the coatings are prepared with an optimum technologic routine [26]. However, in the present work, the same coating parameters were used for these three types of steels. For each steel type, the best aluminide TPBs thus may not have been achieved. As a result, the compactness and integrity of scales (also crucial for coating performance [14]) formed on different steels deviated, which could partly be observed from the section features shown in Figure 6a–c. From this point of view, it can be inferred that the substrates themselves played a part in the formation of aluminide TPBs, resulting in the deviation of deuterium resistance.

On the other hand, although the content of the main alloying element Cr in these three types of Cr steel substrates had an obvious difference, it cannot yet be concluded that Cr is favorable or unfavorable for the deuterium permeation resistance of aluminide TPBs. Therefore, like the formation of Al<sub>2</sub>O<sub>3</sub> scales, the deuterium permeation resistance of aluminide TPBs is not only influenced by the alloying element, but also by other material properties (e.g., crystal or metallographic structure) of steel substrates.

#### 4. Conclusions

The conclusions of this paper are the following:

- The substrate effect presents in the process of Al electrodeposition, exerting an influence on the crystal structure and thickness of Al coatings.
- The steel substrate has an impact on the aluminization process, and the composition and thickness of formed aluminide coatings vary with steel substrates.
- Al<sub>2</sub>O<sub>3</sub> scales formed on different Cr steel substrates exhibit different microstructural features and thicknesses, showing that steel substrates play a role in the process of selective oxidation.
- The deuterium permeation resistance of aluminide TPBs varies with the steel substrate, indicating that the substrate effect is functionalized.

In a word, the steel substrate has an important effect on the formation and deuterium permeation resistance of aluminide TPB coatings. That is, the substrate effect exists in aluminide TPB coatings.

**Author Contributions:** Conceptualization, X.W.; Investigation, X.X., F.Y. and G.Z.; Writing—original draft preparation, X.X.; Writing—review and editing, X.X.; Supervision, X.W.

**Funding:** This research was funded by the National MCF Energy R&D Program (No. 2018YFE0313100).

**Conflicts of Interest:** The authors declare no conflicts of interest.

#### References

1. Hollenberg, G.W.; Simonen, E.P.; Kalinin, G.; Terlain, A. Tritium/hydrogen barrier development. *Fusion Eng. Des.* **1995**, *28*, 190–208. [[CrossRef](#)]
2. Aiello, A.; Ciampichetti, A.; Benamati, G. An overview on tritium permeation barrier development for WCLL blanket concept. *J. Nucl. Mater.* **2004**, *329–333*, 1398–1402. [[CrossRef](#)]

3. Konys, J.; Aiello, A.; Benamati, G.; Giancarli, L. Status of tritium permeation barrier development in the EU. *Fusion Sci. Technol.* **2005**, *47*, 844–850. [[CrossRef](#)]
4. Causey, R.A.; Karnesky, R.A.; Marchi, C.S. Tritium barriers and tritium diffusion in fusion reactors. *Compr. Nucl. Mater.* **2012**, *4*, 511–549. [[CrossRef](#)]
5. Kumar, E.R.; Danani, C.; Sandeep, I.; Chakrapani, C.; Pragash, N.R.; Chaudhari, V.; Rotti, C.; Raole, P.M.; Alphonsa, J.; Deshpande, S.P. Preliminary design of Indian test blanket module for ITER. *Fusion Eng. Des.* **2008**, *83*, 1169–1172. [[CrossRef](#)]
6. Luo, D.; Song, J.; Huang, G.; Chen, C.; Huang, Z.; Deng, X.; Qin, C.; Qian, X.; Zhang, G. Progress of China's TBM tritium technology. *Fusion Eng. Des.* **2012**, *87*, 1261–1267. [[CrossRef](#)]
7. Wong, C.P.C.; Salavy, J.F.; Kim, Y.; Kirillov, I.; Kumar, E.R.; Morley, N.B.; Tanaka, S.; Wu, Y.C. Overview of liquid metal TBM concepts and programs. *Fusion Eng. Des.* **2008**, *83*, 850–857. [[CrossRef](#)]
8. Pedraza, F.; Boulesteix, C.; Proy, M.; Lasanta, I.; de Miguel, T.; Illana, A.; Pérez, F.J. Behavior of slurry aluminized austenitic stainless steels under steam at 650 and 700 °C. *Oxid. Met.* **2017**, *87*, 443–454. [[CrossRef](#)]
9. Serra, E.; Kelly, P.J.; Ross, D.K.; Arnell, R.D. Alumina sputtered on MANET as an effective deuterium permeation barrier. *J. Nucl. Mater.* **1998**, *257*, 194–198. [[CrossRef](#)]
10. Han, S.; Li, H.; Wang, S.; Jiang, L.; Liu, X. Influence of silicon on hot-dip aluminizing process and subsequent oxidation for preparing hydrogen/tritium permeation barrier. *Int. J. Hydrogen Energy* **2010**, *35*, 2689–2693. [[CrossRef](#)]
11. Glasbrenner, H.; Nold, E.; Voss, Z. The influence of alloying elements on the hot-dip aluminizing process and on the subsequent high-temperature oxidation. *J. Nucl. Mater.* **1997**, *249*, 39–45. [[CrossRef](#)]
12. Cheng, W.J.; Wang, C.J. Microstructural evolution of intermetallic layer in hot-dipped aluminide mild steel with silicon addition. *Surf. Coat. Technol.* **2011**, *205*, 4726–4731. [[CrossRef](#)]
13. Ahmadi, H.; Li, D.Y. Mechanical and tribological properties of aluminide coating modified with yttrium. *Surf. Coat. Technol.* **2002**, *161*, 210–217. [[CrossRef](#)]
14. Xiang, X.; Wang, X.L.; Zhang, G.K.; Tang, T.; Lai, X.C. Preparation technique and alloying effect of aluminide coatings as tritium permeation barriers: A review. *Int. J. Hydrogen Energy* **2015**, *40*, 3697–3707. [[CrossRef](#)]
15. Mollard, M.; Pedraza, F.; Bouchaud, B.; Montero, X.; Galetz, M.C.; Schütze, M. Influence of the superalloy substrate in the synthesis of the Pt-modified aluminide bond coat made by slurry. *Surf. Coat. Technol.* **2015**, *270*, 102–108. [[CrossRef](#)]
16. Glasbrenner, H.; Stein-Fechner, K.; Konys, J. Scale structure of aluminized Manet steel after HIP treatment. *J. Nucl. Mater.* **2000**, *283–287*, 1302–1305. [[CrossRef](#)]
17. Li, S.; He, D.; Liu, X.; Wang, S.; Jiang, L. Deuterium permeation of amorphous alumina coating on 316L prepared by MOCVD. *J. Nucl. Mater.* **2012**, *420*, 405–408. [[CrossRef](#)]
18. Oyaidzu, M.; Isobe, K.; Nakamura, H.; Hayashi, T.; Yamanishi, T. Permeation behavior of tritium through F82H steel. *J. Nucl. Mater.* **2011**, *417*, 1143–1146. [[CrossRef](#)]
19. Chen, X.; Huang, Q.; Yan, Z.; Song, Y.; Liu, S.; Jiang, Z. Preliminary study of HDA coating on CLAM steel followed by high temperature oxidation. *J. Nucl. Mater.* **2013**, *442*, S597–S602. [[CrossRef](#)]
20. Lucon, E. Mechanical tests on two batches of oxide dispersion strengthened RAFM steel (EUROFER97). *Fusion Eng. Des.* **2002**, *61*, 683–689. [[CrossRef](#)]
21. Castañeda, S.I.; Bolívar, F.J.; Pérez, F.J. Study of oxyhydroxides formation on P91 ferritic steel and CVD-FBR coated by Al in contact with Ar + 40% $\text{H}_2\text{O}$  at 650 °C by TG-mass spectrometry. *Oxid. Met.* **2010**, *74*, 61–78. [[CrossRef](#)]
22. Kikuchi, K.; Rivai, A.K.; Saito, S.; Bolind, A.M.; Kogure, A. HCM12A oxide layer investigation using scanning probe microscope. *J. Nucl. Mater.* **2012**, *431*, 120–124. [[CrossRef](#)]
23. Sánchez, L.; Bolívar, F.J.; Hierro, M.P.; Pérez, F.J. Temperature dependence of the oxide growth on aluminized 9–12%Cr ferritic-martensitic steels exposed to water vapour oxidation. *Thin Solid Films* **2009**, *517*, 3292–3298. [[CrossRef](#)]
24. Soliman, H.M.; Mohamed, K.E.; Abd El-Azim, M.E.; Hammad, F.H. Oxidation resistance of the aluminide coating formed on carbon steels. *J. Mater. Sci. Technol.* **1997**, *13*, 383–388.
25. Zhang, G.K.; Chen, C.A.; Luo, D.L.; Wang, X.L. An advance process of aluminum rich coating as tritium permeation barrier on 321 steel workpiece. *Fusion Eng. Des.* **2012**, *87*, 1370–1375. [[CrossRef](#)]
26. Forcey, K.S.; Ross, D.K.; Wu, C.H. The formation of hydrogen permeation barriers on steels by aluminizing. *J. Nucl. Mater.* **1991**, *182*, 36–51. [[CrossRef](#)]

27. Fazio, C.; Stein-Fechner, K.; Serra, E.; Glasbrenner, H.; Benamati, G. Investigation on the suitability of plasma sprayed Fe-Cr-Al coatings as tritium permeation barrier. *J. Nucl. Mater.* **1999**, *273*, 233–238. [[CrossRef](#)]
28. Parvathavarthini, N.; Prakash, U.; Dayal, R.K. Effect of carbon addition on hydrogen permeation in an Fe<sub>3</sub>Al-based intermetallic alloy. *Intermetallics* **2002**, *10*, 329–332. [[CrossRef](#)]
29. Fedorov, V.V.; Zasadnyi, T.M.; Korolyuk, R.I.; Balyts'Ky, O.O. Hydrogen permeability of proton-irradiated reactor steels with oxide films. *Mater. Sci.* **2000**, *36*, 701–706. [[CrossRef](#)]
30. Krauss, W.; Konys, J.; Holstein, N.; Zimmermann, H. Al-based anti-corrosion and T-permeation barrier development for future DEMO blankets. *J. Nucl. Mater.* **2011**, *417*, 1233–1236. [[CrossRef](#)]
31. Pedraza, F.; Gómez, C.; Carpintero, M.C.; Hierro, M.P.; Pérez, F.J. On the aluminisation of stainless steel by CVD in fluidised beds. *Surf. Coat. Technol.* **2005**, *190*, 223–230. [[CrossRef](#)]
32. Zhang, G.K.; Li, J.; Chen, C.A.; Dou, S.P.; Ling, G.P. Tritium permeation barrier-aluminized coating prepared by Al-plating and subsequent oxidation process. *J. Nucl. Mater.* **2011**, *417*, 1245–1248.
33. Jamnapara, N.I.; Mukherjee, S.; Khanna, A.S. Phase transformation of alumina coating by plasma assisted tempering of aluminized P91 steels. *J. Nucl. Mater.* **2015**, *464*, 73–79. [[CrossRef](#)]
34. Cheng, W.J.; Liao, Y.J.; Wang, C.J. Effect of nickel pre-plating on high-temperature oxidation behavior of hot-dipped aluminide mild steel. *Mater. Charact.* **2013**, *82*, 58–65. [[CrossRef](#)]
35. Grégoire, B.; Bonnet, G.; Pedraza, F. Reactivity of Al–Cr microparticles for aluminizing purposes. *Intermetallics* **2017**, *81*, 80–89. [[CrossRef](#)]
36. Chen, K.M.; Tsai, D.A.; Liao, H.C.; Chen, I.G.; Hwang, W.S. Investigation of Al–Cr alloy targets sintered by various powder metallurgy methods and their particle generation behaviors in sputtering process. *J. Alloys Compd.* **2016**, *663*, 52–59. [[CrossRef](#)]
37. Cheng, W.J.; Wang, C.J. Effect of chromium on the formation of intermetallic phases in hot-dipped aluminide Cr–Mo steels. *Appl. Surf. Sci.* **2013**, *277*, 139–145. [[CrossRef](#)]
38. Naoi, D.; Kajihara, M. Growth behavior of Fe<sub>2</sub>Al<sub>5</sub> during reactive diffusion between Fe and Al at solid-state temperatures. *Mater. Sci. Eng. A* **2007**, *459*, 375–382. [[CrossRef](#)]
39. Bartur, M.; Nicolet, M.A. Chromium as a diffusion barrier between nickel silicide (NiSi), palladium silicide (Pd<sub>2</sub>Si), or platinum silicide (PtSi) and aluminum. *Cheminform* **1984**, *15*. [[CrossRef](#)]
40. Ruoff, A.L.; Balluffi, R.W. On strain-enhanced diffusion in metals. III. Interpretation of recent experiments. *J. Appl. Phys.* **1963**, *34*, 2862–2872. [[CrossRef](#)]
41. Brune, H.; Bromann, K.; Röder, H.; Kern, K.; Jacobsen, J.; Stoltze, P.; Jacobsen, K.; Nørskov, J. Effect of strain on surface diffusion and nucleation. *Phys. Rev. B* **1995**, *52*, R14380. [[CrossRef](#)]
42. Knorr, D.B.; Rodbell, K.P. Effects of texture, microstructure, and alloy content on electromigration of aluminum-based metallization. In *Proceedings SPIE 1805, Submicrometer Metallization: Challenges, Opportunities, and Limitations*; SPIE: Bellingham, WA, USA, 21 May 1993.
43. Zhang, G.K.; Wang, X.L.; Yang, F.L.; Shi, Y.; Song, J.F.; Lai, X.C. Energetics and diffusion of hydrogen in hydrogen permeation barrier of  $\alpha$ -Al<sub>2</sub>O<sub>3</sub>/FeAl with two different interfaces. *Int. J. Hydrogen Energy* **2013**, *38*, 7550–7560. [[CrossRef](#)]
44. Auinger, M.; Müller-Lorenz, E.M.; Rohwerder, M. Modelling and experiment of selective oxidation and nitridation of binary model alloys at 700 °C-The systems Fe, 1 wt % {Al, Cr, Mn, Si}. *Corros. Sci.* **2015**, *90*, 503–510. [[CrossRef](#)]
45. Borodin, S.; Vogel, D.; Swaminathan, S.; Rohwerder, M. Direct in-situ investigation of selective surface oxidation during recrystallization annealing of a binary model alloy. *Oxid. Met.* **2016**, *85*, 51–63. [[CrossRef](#)]
46. Rупpi, S. Deposition, microstructure and properties of texture-controlled CVD  $\alpha$ -Al<sub>2</sub>O<sub>3</sub> coatings. *Int. J. Refract. Met. Hard Mater.* **2005**, *23*, 306–316. [[CrossRef](#)]
47. Zhang, Z.G.; Gesmundo, F.; Hou, P.Y.; Niu, Y. Criteria for the formation of protective Al<sub>2</sub>O<sub>3</sub> scales on Fe–Al and Fe–Cr–Al alloys. *Corros. Sci.* **2006**, *48*, 741–765. [[CrossRef](#)]
48. Tortorici, P.C.; Dayananda, M.A. Phase formation and interdiffusion in Al-clad 430 stainless steels. *Mater. Sci. Eng. A* **1998**, *244*, 207–215. [[CrossRef](#)]

